Modelling and Simulation in Materials Science and Engineering

PAPER

A three-dimensional realistic microstructure model of particle-reinforced metal matrix composites

To cite this article: X X Zhang *et al* 2014 *Modelling Simul. Mater. Sci. Eng.* **22** 035010

View the article online for updates and enhancements.

Related content

- Computer simulated heterogeneous microstructures
H Singh, Y Mao, A Sreeranganathan et al.
- Mote3D: An open-source toolbox for modelling periodic random particulate microstructures
Henning Richter
- Effect of material inhomogeneity on the cyclic plastic deformation behavior at the microstructural level: micromechanics-based modeling of dual-phase steel
Surajit Kumar Paul

Recent citations

- A stochastic microstructure model for particle reinforced aluminium matrix composites
K. LOSCH *et al*
- Modeling of the Effective Properties of Metal Matrix Composites Using Computational Homogenization
Jos&#233 *et al*
- Enhanced multiscale modeling of macroscopic and microscopic residual stresses evolution during multi-thermo-mechanical processes
X.X. Zhang *et al*

IOP ebooks™

Bringing you innovative digital publishing with leading voices to create your essential collection of books in STEM research.

Start exploring the collection - download the first chapter of every title for free.

This content was downloaded from IP address 210.72.136.37 on 01/08/2019 at 01:17

IOP Publishing Modelling and Simulation in Materials Science and Engineering

Modelling Simul. Mater. Sci. Eng. **22** (2014) 035010 (21pp) doi:10.1088/0965-0393/22/3/035010

A three-dimensional realistic microstructure model of particle-reinforced metal matrix composites

X X Zhang[1], Q Zhang[1], T Zangmeister[2], B L Xiao[1], H Andrä[2] and Z Y Ma[1]

[1] Shenyang National Laboratory for Materials Science, Institute of Metal Research, Chinese Academy of Sciences, 72 Wenhua Road, Shenyang 110016, People's Republic of China
[2] Fraunhofer Institute for Industrial Mathematics, Fraunhofer-Platz 1, Kaiserslautern 67663, Germany

E-mail: zyma@imr.ac.cn

Received 28 August 2013, revised 5 February 2014
Accepted for publication 10 February 2014
Published 14 March 2014

Abstract

A new and robust methodology is presented for the complete computer simulation of large three-dimensional (3D) microstructures of particle-reinforced metal matrix composites (PRMMCs), by integrating the boundary representation scheme, the random cutting algorithm and the random sequential adsorption algorithm. The methodology allows large realistic 3D microstructure models to be generated that can be used for multi-scale investigation of PRMMC structure and design. The effect of the simulation parameters on the simulated microstructure is investigated by applying a quantitative metallographic analysis of the distribution functions of aspect ratio, diameter and the area of reinforcements. Simulated large realistic homogenous 3D microstructures of PRMMC are in close agreement with the experimental microstructures.

Keywords: metal matrix composites, computer simulation, modeling, realistic microstructure

(Some figures may appear in colour only in the online journal)

1. Introduction

Particle-reinforced metal matrix composites (PRMMCs) are widely used in advanced structure, energy and information industries due to their distinctive properties, such as high strength, high

stiffness and light weight. These properties result from the multi-scale features and multi-phase structures of PRMMCs. At the micro-scale ($\sim\mu$m scale), PRMMCs are viewed as multi-phase (i.e. matrix and particles) materials. The types of matrix alloys and particles, the heat treatment state of the matrix alloy, the content of the particles, etc. control the macroscopic properties of PRMMCs. At the macro-scale ($\sim$mm scale), PRMMCs are viewed as single-phase (i.e. homogeneous) materials and the macroscopic properties are critical for component and structure design and analysis.

The multi-scale modeling and simulation of PRMMCs can take into account the multi-phase structure and the heterogeneous distribution of physical fields (such as stress field, strain field and electromagnetic field) at the micro-scale, and can provide an optimized structure and design of the materials or components before they are fabricated in reality. The two basic steps involved in multi-scale modeling and simulation of PRMMCs are (i) construction of multi-phase microstructures of PRMMCs, and (ii) microstructure-based computation of macroscopic properties using numerical methods such as finite element (FE) and finite volume (FV) methods. In these steps, the microstructure model plays a primary role.

The microstructure models may be categorized into idealized models, experimental models or simulated realistic models. The idealized models assume that the particles have a simplified shape or are distributed regularly [1–3]. The complex shape or irregular distribution of real particles in PRMMCs is not considered in the idealized models. The experimental realistic models usually employ experimental images of PRMMCs to reconstruct the microstructure. A two-dimensional (2D) experimentally reconstructed model employs one 2D image, while a three-dimensional (3D) experimentally reconstructed model requires serial 2D images. The experimentally reconstructed models can reflect the actual shape, size and distribution of particles in PRMMCs [4–8]. However, owing to the laborious work, the length of the third dimension of a 3D reconstructed microstructure is usually smaller than that of the other two dimensions [5, 8–10]. Recently, the x-ray tomography technique has been applied to reconstruct 3D microstructures of PRMMCs [11–13]. Compared to the method using serial 2D metallographs, the x-ray tomography technique is more efficient and its resolution reaches 1–2 μm [14, 15].

Another method for generating a realistic microstructure is the computer modeling and simulation method. Up to now, numerous computer simulations of PRMMC microstructures have been reported. The main categories include the random sequential adsorption (RSA) algorithm [16–21], Monte Carlo procedures [22, 23] and volume mesh techniques [24, 25]. However, most of these simulations focused on 2D or 3D idealized microstructures, and did not compare the simulated results with experimental data.

In this work, a new and robust methodology is proposed for complete computer simulation of large 3D PRMMC microstructures that can be used for multi-scale investigations of PRMMC structure and design. Since the simulated microstructure is dependent on the simulation algorithm, assessments of the effect of each simulation parameter on the simulated microstructure are crucial. When building the relationship between the algorithm input parameters and the microstructural attributes, such as aspect ratio, diameter and the area of particles, a large realistic 3D PRMMC microstructure is simulated.

2. Background of the solid modeling method

Usually, the microstructure-material property simulation chain is as follows: microstructure model→finite element (FE) or finite volume (FV) mesh→FE/FV modeling/simulation of material properties. In the chain, the microstructure model needs to capture the main attributes

of the real materials, and then has to be divided into FEs or FVs. A flexible and robust tetrahedral mesh library TetGen developed in [26] has been adopted to generate the FE/FV meshes. The main advantage of the tetrahedral mesh is that it can be re-meshed efficiently to improve the mesh quality in the case of large deformations. The general input data structure of TetGen is the piecewise linear complexes (PLC) [27] which can approximately represent any 3D domain by using the set of vertices, segments and facets.

Such a mesh-generation technique requires a compatible solid modeling technique, which provides the geometrical information, such as vertices, edges and faces, so that the solid model can be converted to PLC. Several different techniques can be used for creating or representing solid models. Among them, three prominent solid modeling techniques are the cell decomposition scheme, the constructive solid geometry (CSG) scheme and the boundary representation (BREP) scheme.

The cell decomposition scheme divides the object space into unit-sized elements (usually cubes), and represents shapes as sets of these elements. Interfaces and boundaries of the cell decomposition model have step profiles, because the minimal resolution is limited by the size of these unit elements. To obtain a better approximation of interfaces and boundaries, an additional technique is required; for example, the extended finite element method (XFEM) [28] or the immersed interface method (IIM) [29]. The geometry model created by the cell decomposition method can be divided into a regular voxel mesh. Unfortunately, it is not suitable for free unstructured mesh subdividing.

The CSG scheme creates a complex surface or object by using Boolean operations to combine the primitives, which are the simplest objects, such as cuboids, cylinders and spheres. The two main parts of the CSG technique are the primitives, which are described by size parameters and orientation parameters, and Boolean operations, which indicate how to build the CSG model from the primitives. The CSG model can be discretized by free unstructured meshes. However, the fundamental and topological character of the CSG model is that it does not store the geometrical information explicitly. Therefore, if the CSG model is used for mesh generation, the geometry information can only be evaluated by additional algorithms.

Unlike the cell decomposition and CSG scheme, the BREP scheme represents shapes using their limits. A BREP model is described by topology (the structure of the object with vertices, edges and faces as the main items) and geometry (the form of the object; i.e. points, curves and surfaces). The BREP technique is particularly suitable for mesh generation using PLC, because the BREP model explicitly contains the geometry information. Therefore, the BREP technique is applied as the fundamental technique for computer simulation of PRMMC microstructure in this study.

The corresponding data structure of the BREP technique that has been well defined in [30] is used in the present work. The framework of 3D Euclidean space is applied for the microstructure modeling.

3. 3D microstructure model

To reduce the complexity of the modeling algorithm, yet reproduce the main features of a real PRMMC microstructure, we simulate the realistic microstructure. Reinforcements, such as SiC, Al_2O_3 and B_4C particles, are assumed to have convex shapes with planar sides so that they can be defined as bounded convex polyhedrons rather than real complex shapes. An object-orientated computer program has been written in C++. The algorithms of the microstructure generating technique are composed of two parts: (i) the generation of arbitrary polyhedrons; and (ii) the placement of random polyhedrons at random positions in a representative volume

element (RVE). Boolean operations are used to generate random polyhedrons, and the RSA algorithm is applied to locate the polyhedrons randomly within an RVE. The details of the microstructure generating technique are described in sections 3.1 and 3.2.

3.1. Generation of random polyhedrons

A novel algorithm has been developed to capture the random shapes and sizes of reinforcements in PRMMC, for modeling a realistic microstructure of PRMMC. Arbitrary convex polyhedrons are used to represent the random reinforcements in this study. A Boolean-operation-based technique, called a cutting process, is proposed for generating random convex polyhedrons.

Local Euclidean coordinates are used for the cutting process. An arbitrary convex polyhedron is generated by using several planes to cut a primitive object. The primary substep is to generate a primitive object. This should be simple so that it is easy to implement using the BREP technology, and should have one or several fundamental attribute(s) of the real reinforcement. According to these conditions, a cuboid that is defined by a triple (A, B, C) indicating its length A, width B and height C, with its center point located at the origin $\boldsymbol{O}$ in the local Euclidean coordinates, is applied as the primitive object in this work. It is easy to use the BREP technique for the computer description of such a cuboid. Furthermore, a real reinforcement in PRMMC can be classified into sphere-approximated or ellipsoid-approximated particles, if one considers the minimum convex hull of the reinforcement. A cuboid also has such an attribute. Its minimum convex hull may be a sphere or an ellipsoid, depending on whether $A = B = C$.

In order to form an arbitrary convex polyhedron, the cuboid basis is then cut by several planes. In the present study, a plane in a 3D local Euclidean coordinate system is defined by $\boldsymbol{H}(\boldsymbol{P}, \boldsymbol{N})$, which states a plane $\boldsymbol{H}$ that passes through point $\boldsymbol{P}$ and has an orthogonal direction equal to $\boldsymbol{N}$. Point $\boldsymbol{P}$ is simulated at a uniformly distributed random position within the cuboid for the sake of simplicity. Generally, the direction $\boldsymbol{N}$ and the vector $\boldsymbol{OP}$ are independent of each other. In other words, the direction $\boldsymbol{N}$ can be either parallel to the vector $\boldsymbol{OP}$ or not. Based on these two relationships between the direction $\boldsymbol{N}$ and the vector $\boldsymbol{OP}$, two types of cutting planes are defined and used in the present work. The first type of plane has only one governing parameter since the orthogonal direction $\boldsymbol{N}$ is parallel to the vector $\boldsymbol{OP}$, in other words, the orthogonal direction of the plane is associated with the position of that plane. Hence, the first type of plane is called a random position–associated direction-plane (RPADP). The second type of plane has two governing parameters whereby both the position $\boldsymbol{P}$ and the orthogonal direction $\boldsymbol{N}$ are simulated as uniformly distributed random variables. Hence, the second type of plane is called a random position–random direction-plane (RPRDP). Figure 1 illustrates the two cutting processes using RPADP and RPRDP.

The effects of the RPADPs and RPRDPs on the geometry attributes of generated arbitrary convex polyhedrons are investigated in the present work and discussed in section 5.3. Further quantitative analysis of the cutting process is necessary to control the size and shape of random particles. Therefore, two simulation parameters are introduced, based on the simulation algorithm for generating arbitrary convex polyhedrons. They are as follows. α: original aspect ratio of the primitive object. It is defined by the following three equations:

$$\alpha = \frac{B}{A}, \tag{1}$$

$$A = C, \tag{2}$$

$$A \times B \times C = \text{const}. \tag{3}$$

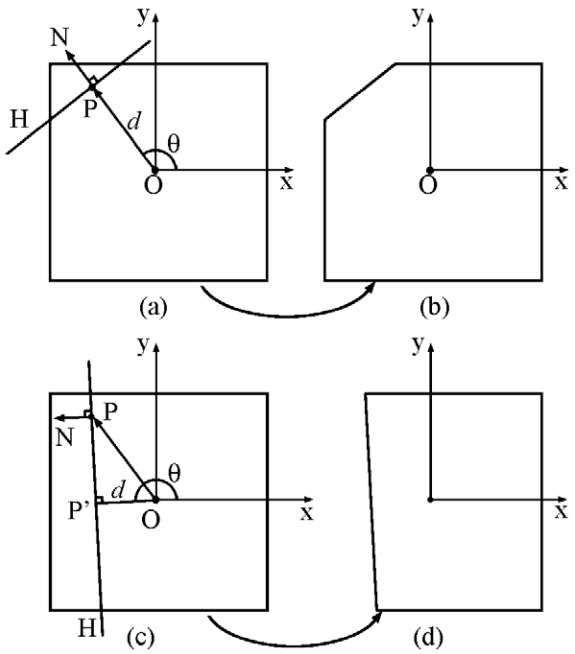

Figure 1. Illustration of cutting process using (*a*), (*b*) RPADP; (*c*), (*d*) RPRDP.

It can be seen that the definition of α is specialized so that the investigation of the attributes and performance of the simulation algorithm can be simplified. Note that, if necessary, a more complex original aspect ratio, where $A \neq B \neq C$ is considered, can also be used in this algorithm.

$\boldsymbol{K}$: Ratio of RPRDPs. It is defined by

$$\boldsymbol{K} = \frac{\text{Number of RPRDPs}}{\text{Total number of cutting planes}}. \tag{4}$$

Once a polyhedron is formed, a filter criterion is applied, to check whether the shape of the polyhedron is admissible. A so-called minimum edge length criterion is proposed to avoid a polyhedron with too-small edges. If there is a too-small edge, the corresponding mesh discretization will be very dense around the edge, which raises the numerical computation cost directly and may introduce a large numerical error in the material property simulation. Finally, figure 2 shows the flow chart that summarizes the generation process of arbitrary polyhedrons.

3.2. Placing polyhedrons in random positions

The RSA algorithm is widely used for investigating particle-reinforced composites [17, 18, 21] or fiber-reinforced composites [20, 31–33]. The main idea of the RSA algorithm is to try to place a particle at a position in a specified volume if the particle satisfies user-defined conditions, or trying a new position if the particle does not satisfy user-defined conditions.

In the present work, an arbitrary convex polyhedron, generated according to the previous step, is added to a 3D microstructure box, using the RSA algorithm. Penetration or contact between any two polyhedrons is not admissible in the present work. Besides, a geometrical periodicity condition can be employed.

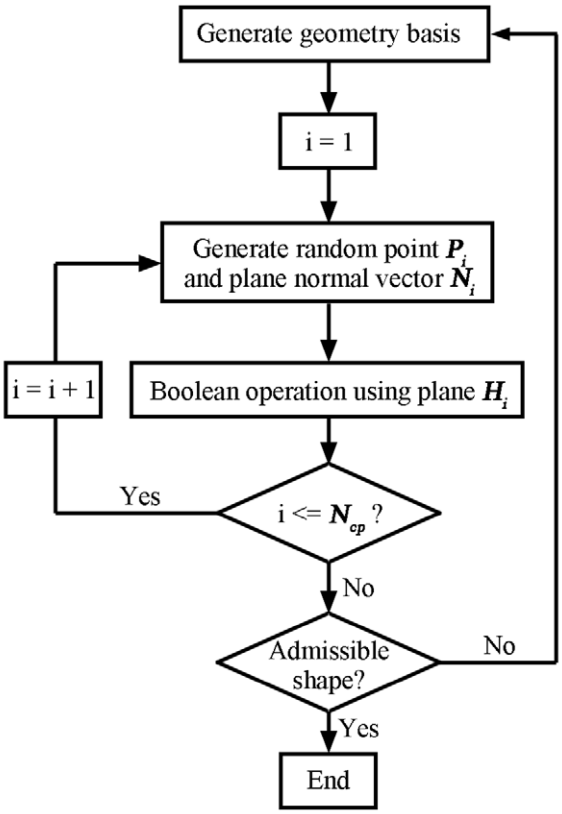

Figure 2. Flow chart of the generation of random convex polyhedron.

Once a new particle is accepted, the solid volume fraction (SVF) of the added particles is updated. This sequential adding process repeats until a target SVF (i.e. the volume fraction of particles in the composite) is satisfied. Figure 3 summarizes the flow chart of the RSA algorithm used in the present work. All simulations run in a ThinkStation-D20 with 2 Xeon 5690 CPUs (3.47 GHz) and 32 GB memory.

4. Experiments

4.1. 2D experimental image of PRMMC microstructure

2009Al-based composites, reinforced by 20 vol% SiC particles with a nominal mean particle diameter of 20 μm, were used in this study. The composition of the 2009Al alloy is Cu 3.8–4.2 wt%, Mg 1.2–1.6 wt% and the remainder is Al. All the composites were fabricated by powder metallurgy (PM) and subsequent hot forging. The Al alloy and SiC powders were blended for 8 h, and then compacted at a pressure of 40 MPa. The compacts were pressed at a pressure of 50 MPa in a vacuum chamber of 10^{-2} Pa, after being held at 580 °C for 60 min (see figure 4(*a*)). The hot pressed billets were forged in an open die, using 200 MPa pressure. The total deformation ratio was 4 : 1. The microstructures of the forged billets were examined by optical microscopy (OM, Axiovert 200 MAT). The sampling location for OM is illustrated in figure 4(*b*).

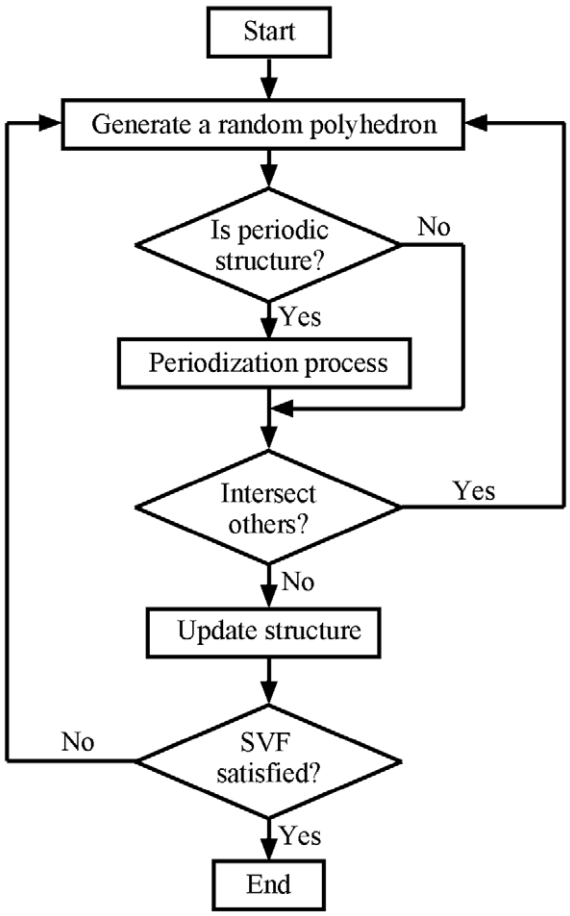

Figure 3. Flow chart of RSA algorithm.

4.2. Simulation of microstructures

The primitive objects are cut by several random planes (RPADPs and RPRDPs). In the simulation, the total number of random planes N_{cp} is empirically set to 10. It should be noted that a primitive object is cut by the first random plane and then the next random plane and so on. The cutting process is random, so some random planes may miss the semi-finished particle and the number of facets of particles is random. The effects of the two simulation parameters α and $\boldsymbol{K}$ with fixed primitive object size on the shape and size of polyhedrons are studied to assess the cutting process in this work. The size of the primitive object is defined by the diameter of the circumscribed sphere of the primitive object. The parameter settings of α and $\boldsymbol{K}$ are shown in table 1 with the diameter of the circumscribed sphere of the primitive object being 20 μm. All the simulated 3D microstructures have the same size of 450 μm. For each simulation, 2D images are obtained by slicing the 3D microstructures. The planes from which the images are sliced are parallel to the the *YOZ*, *XOZ* or *XOY* plane (in the following text the word 'plane' is omitted for simplification when mentioning these special planes), respectively. Simulations 1, 2 and 3 are conducted to explore the microstructure anisotropy, depending on the α of the primitive object. Therefore, statistical parameters are analyzed in

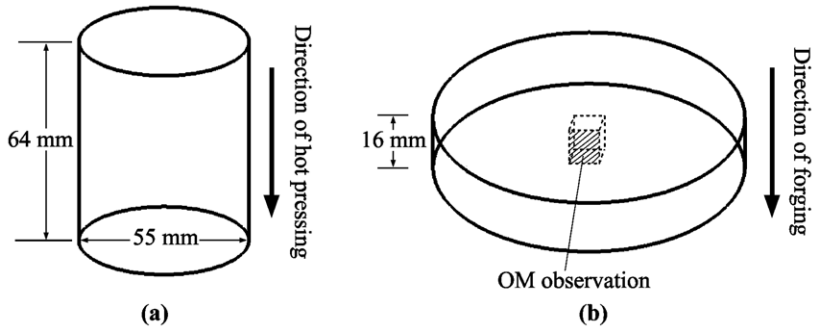

Figure 4. Experimental composite material preparation.

Table 1. The simulation set for the assessment of the cutting process.

Simulation	α	K
1	1.0	0.6
2	2.0	0.6
3	4.0	0.6
4	1.0	0.0
5	1.0	0.5
6	1.0	1.0

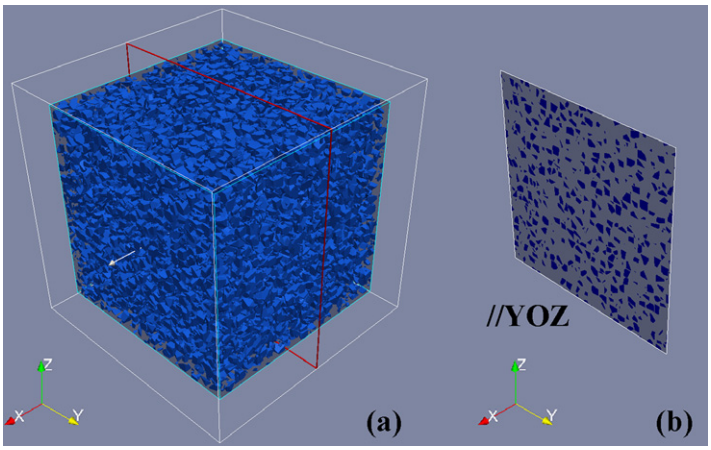

Figure 5. Slicing (*a*) a simulated 3D microstructure to obtain (*b*) a 2D image. The 2D image is in the plane parallel to *YOZ*.

planes parallel to *YOZ*, *XOZ* and *XOY* for simulations 1, 2 and 3. Figure 5 illustrates how to obtain a 2D image in a plane parallel to the *YOZ*. The quantitative metallographic properties—i.e. the area, aspect ratio and diameter of particles—are analyzed for both experimental and simulated microstructure images.

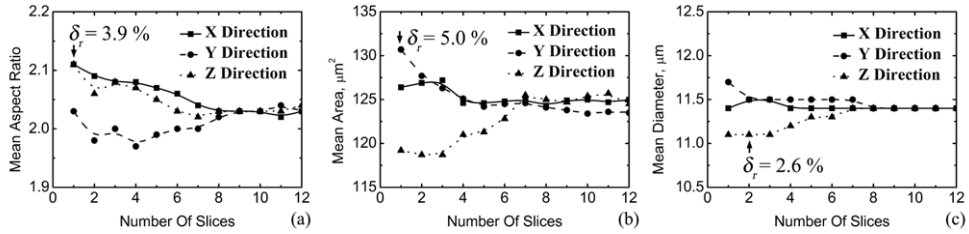

Figure 6. Numerical convergence of statistical parameters with the number of slices in simulation 1: (*a*) mean aspect ratio, (*b*) mean area and (*c*) mean diameter. The largest relative error δ_r is marked for every parameter.

5. Results and discussions

5.1. The number of 2D images to obtain accurate statistical results

One question about the statistical results is whether they are accurate. To obtain accurate statistical results, a large sample size is required. Therefore, one can either use a single large 2D image that contains thousands of particles, or use several medium-sized 2D images, with each of them containing hundreds of particles. The first requires a large 3D microstructure, which may not be the best choice, owing to expensive computational cost. The second requires a medium-sized 3D microstructure, and has been chosen for the present work.

According to the definition of α in section 3.1, if α is 1.0 the geometry primitives are simple cubes that are reformed into random polyhedrons in the cutting process, and then located randomly in the 3D microstructure box using the RSA algorithm. As a result, the attributes of the simulated microstructure should be isotropic. Therefore, theoretically, the statistical parameters in the planes parallel to *YOZ*, *XOZ* and *XOY* should be equal to each other.

Figure 6 illustrates the convergence of the statistical parameters of simulation 1 as the number of 2D images increases. Relatively large errors attach to the statistical results in planes parallel to *YOZ*, *XOZ* and *XOY* when the sections are few. As shown in figure 6(*a*), the larger the number of 2D images, the closer the mean aspect ratios in the planes parallel to *YOZ*, *XOZ* and *XOY* become. When the number of 2D images is equal to, or larger than eight, the relative difference in the mean aspect ratios in the planes parallel to *YOZ*, *XOZ* and *XOY* can be ignored. Figures 6(*b*) and (*c*) show that the number of 2D images to obtain stable values for both mean area and mean diameter is seven. The stable values for the statistical mean aspect ratio, area and diameter are 2.03, 124.5 μm^2 and 11.4 μm, respectively.

The largest relative statistical errors attached to the mean aspect ratio, area and diameter are 3.9%, 5.0% and 2.6% for 1, 1 and 2 sections, respectively. Therefore, the suitable number of 2D images for obtaining stable and precise statistical parameters is eight for simulation 1. If eight is fixed as the number of 2D images for obtaining expected accurate statistical results for all other simulations, the real statistical results may have small errors, since the 3D microstructure is simulated via different parameters. Fortunately, this error may be ignored as the largest statistical error that appears in simulation 1 is 5.0%. In this work, the appropriate number of 2D images is chosen to be ten to obtain the stable and accurate results for every statistical parameter of various simulations.

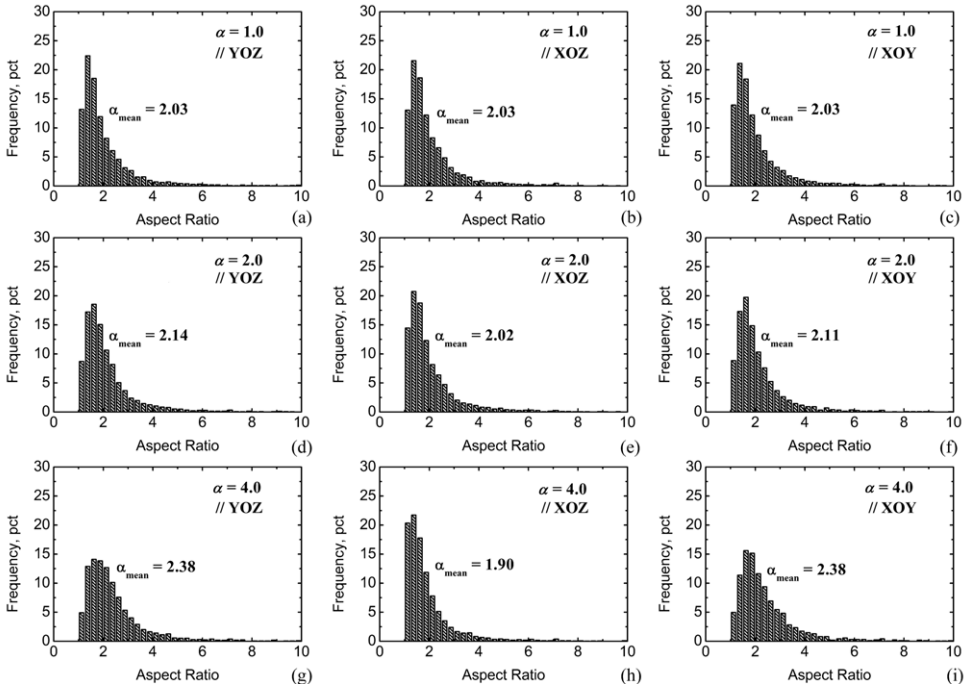

Figure 7. Histograms showing the aspect ratio distribution of the particles of different simulations: (*a*), (*b*) and (*c*) are the results with $\alpha = 1.0$; (*d*), (*e*) and (*f*) the results with $\alpha = 2.0$; (*g*), (*h*) and (*i*) the results with $\alpha = 4.0$. '*//YOZ*', '*//XOZ*' and '*//XOY*' mean in the planes parallel to '*YOZ*', '*XOZ*' and '*XOY*', respectively. $\boldsymbol{N}_{\mathrm{cp}} = 10$ and $\boldsymbol{K} = 0.6$ are applied for all the simulations.

5.2. Effects of the original aspect ratio of the primitive object

Theoretically, according to the definition of α in section 3.1, the attributes of a simulated 3D microstructure in the planes parallel to *YOZ* are expected to equal those in the planes parallel to *XOY*. Especially if α equals 1.0, the 3D microstructure should be isotropic. Otherwise, if the rotational degree of freedom (DOF) is not activated in the RSA, the simulated 3D microstructure should be transversally isotropic. In the present paper, in order to access the effects of the original aspect ratio the rotation DOF is not applied.

Figures 7(*a*)–(*c*) show that the histograms of aspect ratio in all three directions are almost the same when α equals 1.0, and the aspect ratio of most particles is in the range between 1.0 and 2.0, with the mean aspect ratio being 2.03. When the primitive object shrinks along the X- and Z-axes and elongates along the Y-axis, α increases. When α is 2.0 (see figures 7(*d*) and (*f*)), in the planes parallel to *YOZ* and *XOY*, the frequency of particles with the aspect ratio in the range between 1.0 and 2.0 increases and that with aspect ratio larger than 2.0 decreases. As a result, the mean aspect ratio increases from 2.03 to 2.14 in the planes parallel to *YOZ*, which agrees approximately with 2.11 in the planes parallel to *XOY*. As shown in figure 7(*e*), when α equals 2.0, the mean aspect ratio in the planes parallel to *XOZ* is slightly smaller than that when α is 1.0. These variational trends are enhanced when α is increased to 4.0. Figures 7(*g*) and (*i*) show that, in the planes parallel to *YOZ* and *XOY*, the peak frequency of particles obviously smoothes out between the aspect ratios of 1.0 and 2.0, and increases when

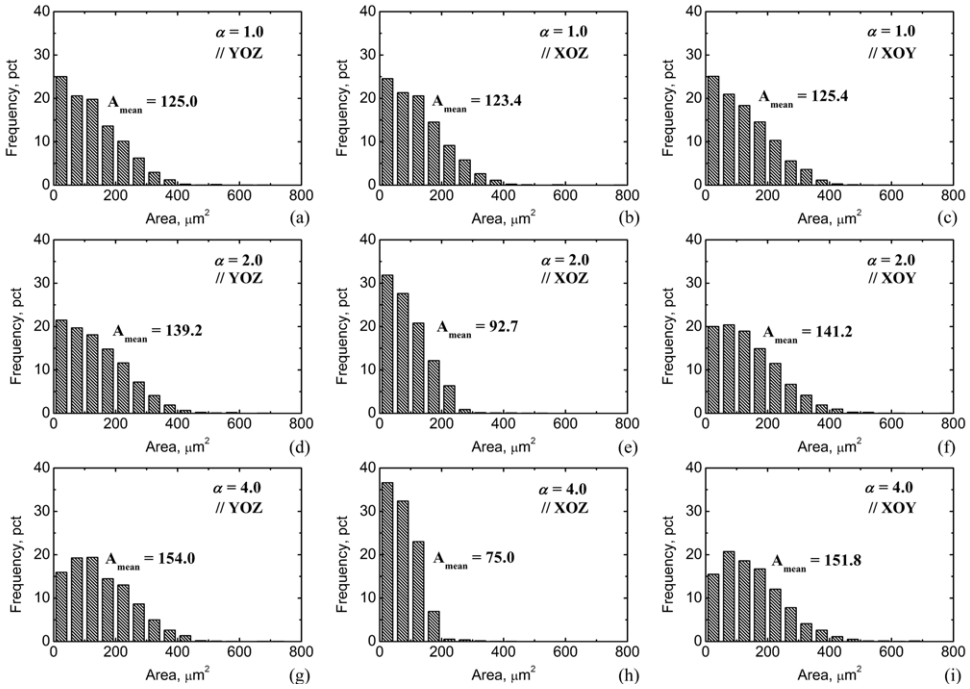

Figure 8. Histograms showing the area statistics of the particles of different simulations with the same simulation parameter setting as in figure 7.

the aspect ratio is larger than 2.0. Consequently, the mean aspect ratios increase to 2.38 in the planes parallel to *YOZ* and *XOY*. In contrast, in the planes parallel to *XOZ*, the peak frequency of particles between the aspect ratios of 1.0 and 2.0 is enhanced, and the mean aspect ratio decreases to 1.90, as shown in figure 7(*h*). These results reveal that as the original aspect ratio of the primitive object increases, the frequency of particles with large aspect ratios increases in the planes perpendicular to the shrinking directions of the primitive object (i.e. parallel to the X- and Z-axes in the present work), whereas it decreases in the planes perpendicular to the elongated direction of the primitive object (i.e. parallel to the Y-axis).

Figures 8(*a*)–(*c*) confirm that the area distributions in all three directions are the same when α equals 1.0, and that the area of most particles is in the range between 0 and 200.0 μm^2. The frequency of particles decreases continuously with an increase in area. When α increases to 2.0, in the planes parallel to *YOZ* and *XOY*, the frequency of particles with areas of 0–200.0 μm^2 decreases slightly, but it increases a little for areas larger than 200.0 μm^2, with the mean area increasing from $\sim$125.0 to $\sim$140.0 μm^2. In the planes parallel to *XOZ*, the frequency of particles with areas of 0–200.0 μm^2 increases obviously, and decreases when the area is larger than 200.0 μm^2. Hence, the mean area decreases to 92.7 μm^2 in the planes parallel to *XOZ*. When α increases further to 4.0, the variation trends in different directions are enhanced. As a consequence, the mean area increases to $\sim$154.0 μm^2 in the planes parallel to *YOZ* and *XOY*, whereas it decreases to 75.0 μm^2 in the planes parallel to *XOZ*. From these results, it is revealed that as the original aspect ratio of primitive objects increases, the frequency of particles with large areas increases in the planes perpendicular to the shrinking directions of the primitive object, i.e. parallel to the $X-$ and Z-axes in the present work, whereas it decreases in planes perpendicular to the elongated direction of the primitive object, i.e. parallel to the Y-axis.

Table 2. Number of particles of each simulation.

Simulation	Number of particles
1	8543
2	8893
3	9747
4	4334
5	7486
6	16390

These variational trends can be explained with help from the definition of α and equations (1)–(3). The volume of a primitive is assumed to be unitary; i.e.

$$A \times B \times C = 1.0. \tag{5}$$

In order to simplify the explanations, let A and C equal x, then B can be calculated by αx. It is easy to find that

$$\alpha x^3 = 1.0, \tag{6}$$

then one can easily obtain

$$S = \alpha x^2 = \alpha^{1/3}. \tag{7}$$

This simple function reflects that the side area of the primitive object increases by increasing the original aspect ratio. If α increases twice—that is, from 1.0 to 2.0, or from 2.0 to 4.0—y will increase by $\sqrt[3]{2}$ (i.e. about 1.3) times. The result plotted in figure 8 shows that the area in the planes parallel to *XOY* increases by about 1.1 times (i.e. 139.2/125.0 when α increases from 1.0 to 2.0), which reveals that the area increase of the final random polygon, i.e. the section of polyhedron, is smaller than that of the original side area. This phenomenon corresponds to the variation of the total number of particles contained in the whole 3D microstructure. Table 2 shows that the number of particles in the simulated 3D microstructure increases with increasing α, which means that the average volume of each particle decreases when α increases. In other words, the larger α is, the larger the volume is cut away.

Figure 9 shows that the statistical mean diameter increases in the planes parallel to *YOZ* and *XOY*, and decreases in the planes parallel to *XOZ* when α increases. This can be understood easily with the help of the relationship between diameter and area. Generally, the relationship between the diameter a in the planes parallel to the *YOZ* and *XOY* and the area S can be written as

$$a \propto S^{1/2}. \tag{8}$$

According to equation (7), it is easy to get

$$a \propto \alpha^{1/6}. \tag{9}$$

Equation (9) indicates that if the model is self-consistent, the mean diameter in planes parallel to the *YOZ* and *XOY* increases with increasing α.

5.3. Effects of the ratio of RPRDPs

Figure 10 illustrates the effects of $\boldsymbol{K}$ on the microstructure attributes. By increasing $\boldsymbol{K}$ from 0 to 1.0, as shown in figures 10(*a*)–(*c*), the frequency of particles with large aspect ratios increases, and the mean aspect ratio increases from 1.68 to 2.21. Figures 10(*d*)–(*f*) show that

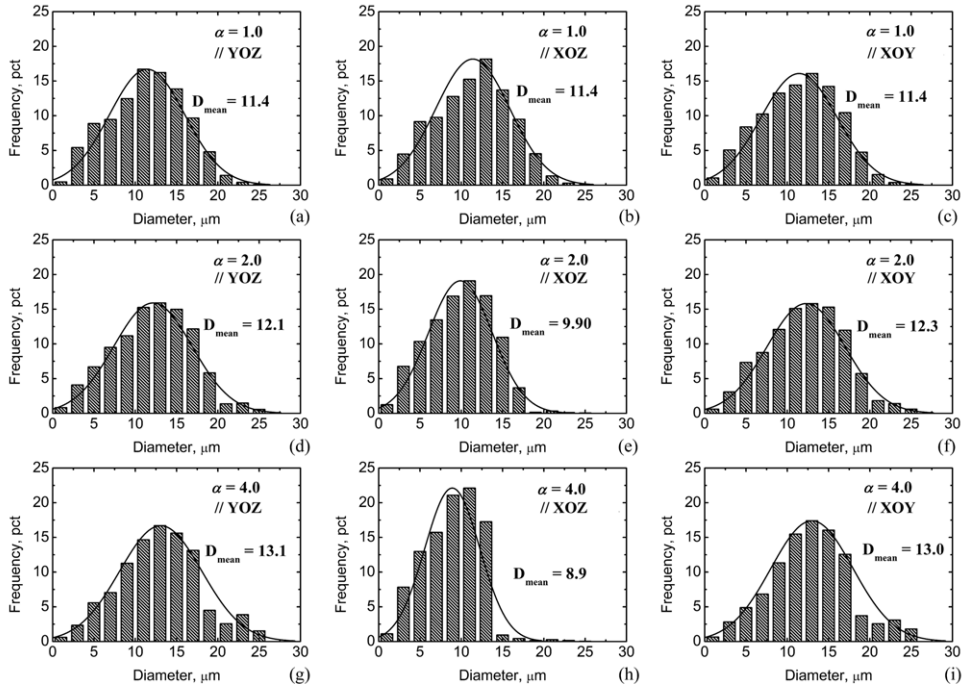

Figure 9. Histograms showing the diameter statistics of the particles of different simulations with the same simulation parameter setting as in figure 7.

the frequency of particles with small areas (or small sizes) clearly increases as $\boldsymbol{K}$ increases, with the mean area decreasing from 208.5 to 79.6 μm^2. It can be seen that both the value and the pattern of the area distribution are sensitive to $\boldsymbol{K}$. Figures 10(g)–(i) confirm that the frequency of particles with small diameters (or small sizes) clearly increases as $\boldsymbol{K}$ increases, with the mean diameter decreasing from 15.2 to 9.0 μm.

An inspection of these results reveals that the microstructure is strongly dependent on $\boldsymbol{K}$. According to the definition, the larger $\boldsymbol{K}$ is, the more RPRDPs and fewer RPADPs are used to cut the primitive object. Therefore, the effects of $\boldsymbol{K}$ are a result of the different effects of the RPRDPs and the RPADPs. It should be noted that the first kind of plane is a particular case of the second kind of plane, because the random direction $\boldsymbol{N}$ of the second kind of plane has an infinitesimal probability of being parallel to the vector $\boldsymbol{OP}$. In the present work, each polyhedron is generated by the cutting process with, at most, ten cutting planes. Even if all the cutting planes are random planes, the probability that the random direction $\boldsymbol{N}$ is parallel to the vector $\boldsymbol{OP}$, which is, at most, 10 times infinitesimal, is still an infinitesimal, and can be ignored. Hence, these two types of planes do differ. Furthermore, if the distance d (as shown in figure 1) between the local origin point $\boldsymbol{O}(0, 0, 0)$ and the cutting plane is considered, the different effects of these two kinds of cutting planes are obvious. It is easy to obtain the following relationship:

$$d_{\mathrm{RPADP}} \geqslant d_{\mathrm{RPRDP}}, \tag{10}$$

which suggests that the second kind of plane may cut away more volume of the primitive, because it is closer to the center of the primitive object. As shown in figure 1, if the two cutting planes pass through the same position, the RPRDPs are closer to the local origin point than the

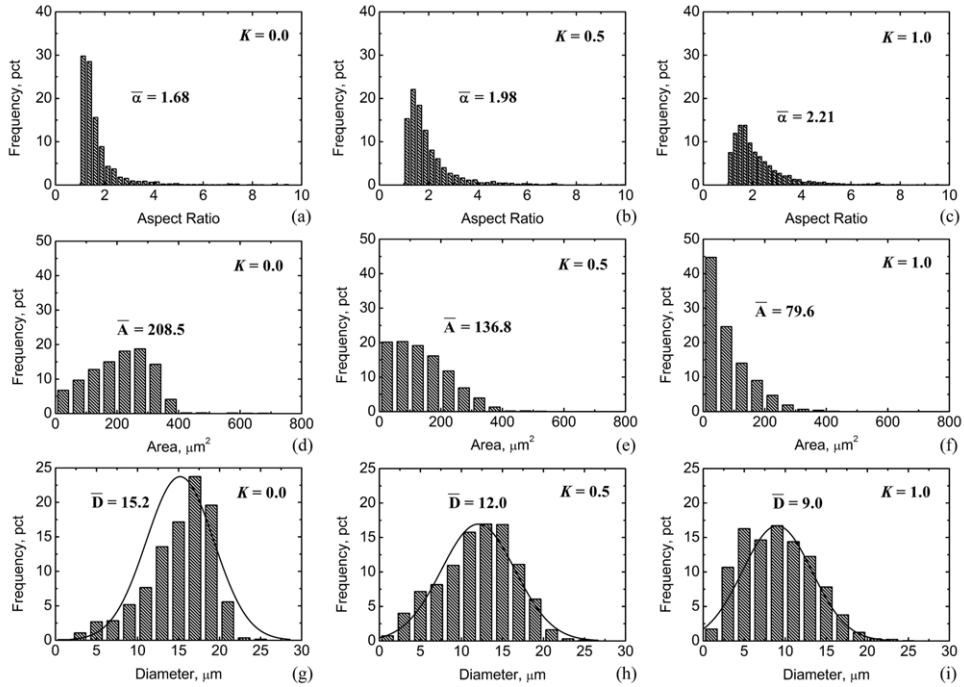

Figure 10. Effects of $\boldsymbol{K}$ on the statistical parameters of slices whose parent RVEs are generated with $N_{\mathrm{cp}} = 10$ and $\alpha = 1.0$: (*a*), (*b*), (*c*) aspect ratio; (*d*), (*e*), (*f*) diameter; (*g*), (*h*), (*i*) area.

Table 3. Simulation sets for constructing the 3D realistic microstructure.

			Fraction of geometry primitives		
Microstructure	α	$\boldsymbol{K}$	20 μm	10 μm	5 μm
S1	1.0	0.6	0.900	0.090	0.010
S2	1.0	0.6	0.900	0.080	0.020
S3	1.0	0.6	0.900	0.070	0.030

RPADPs, and the retained shape becomes more elongated. It explains why as $\boldsymbol{K}$ increases, i.e. the number of the RPRDPs increases, the average particle size decreases, while the aspect ratio increases.

5.4. Generation of a realistic microstructure

In the present work, two simulation parameters of the cutting process have been investigated. The simulated results show that both α and $\boldsymbol{K}$ affect the sizes and shapes of the arbitrary convex polyhedrons. In this part, a realistic PRMMC microstructure is simulated by introducing a third parameter; i.e. the diameter distribution function of the primitive object.

Three sets of simulation parameters are studied, as summarized in table 3. The preparation of material for the experiment has been described in section 3.1. In order to obtain the accurate statistical parameters of the experimental material, the convergence of the statistical parameters

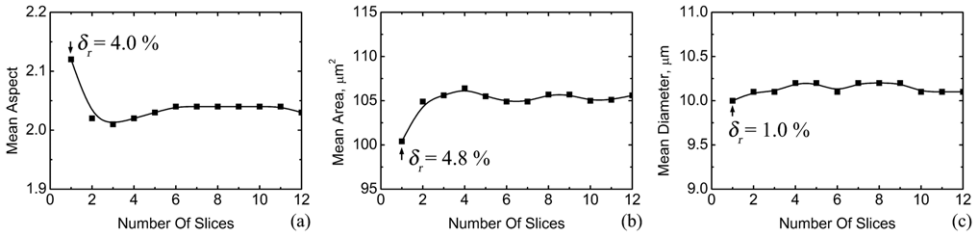

Figure 11. Statistic convergence of (*a*) the mean aspect, (*b*) the mean area and (*c*) the mean diameter with the number of slices in the experimental microstructure. The largest relative error δ_r is marked for every parameter.

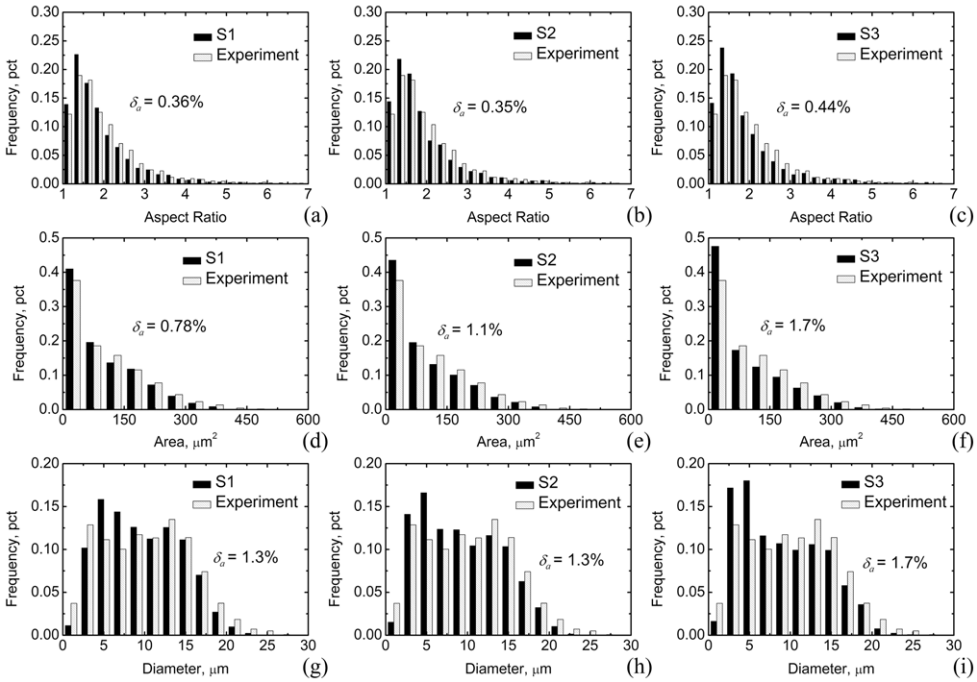

Figure 12. Comparison between simulated microstructure and experimental microstructure using statistical histogram of (*a*), (*b*), (*c*) aspect ratio; (*d*), (*e*), (*f*) area and (*g*), (*h*), (*i*) diameter. The statistical error δ_a is marked for every parameter.

of the SiC PRMMC material is investigated, and shown in figure 11. The plotted results reveal that five sections are enough to obtain stable and accurate statistical parameters. The convergence of the statistical parameters is required not only for the experimental material, but also for the simulations. To be consistent, 10 sections that have been used for all the previously simulated microstructures are again applied for simulations S1 to S3 and the experiment.

A comparison of the aspect ratio, area and diameter distribution functions between the simulations and experiment is plotted in figure 12. A statistical error δ_a is introduced to assess the accuracy of the simulations. δ_a is computed by integrating the absolute difference in each bar of the frequency chart between the simulation and the experiment and then divided by the number of bars. It can be observed that simulation S2 is the best approximation (figure 12). In addition, by increasing the content of small primitives, the aspect ratio distribution of

Table 4. Comparison of mean particle number density between different simulations and the experiment.

Microstructure	Mean particle number density (mm^{-2})	Relative error
Experiment	2141	—
Simulation S1	2014	5.9%
Simulation S2	2173	1.5%
Simulation S3	2277	6.4%

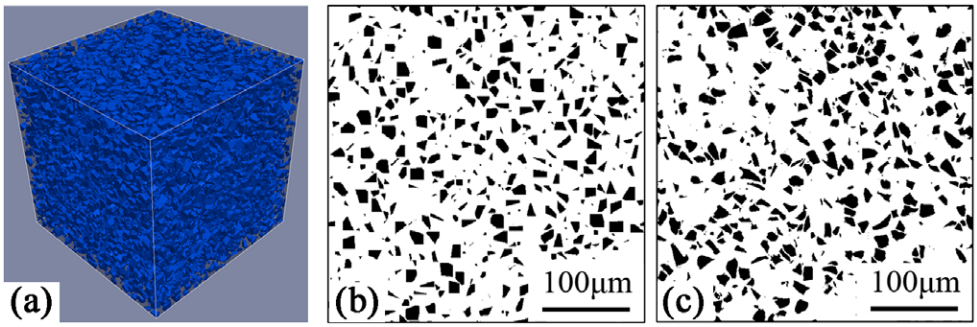

Figure 13. Microstructures of a 20 μm 20 vol% SiC_p/Al composite: (*a*) simulated large 3D microstructure which is 450 μm^3 large and has 22075 SiC particles. The simulation time takes 6699 s in a ThinkStation-D20 with 2 Xeon 5690 CPUs (3.47 GHz) and 32 GB memory; (*b*) a 2D image sliced from (*a*); (*c*) segmental 2D image of the experimental microstructure.

simulated particles varies slightly, as shown in figures 12(*a*)–(*c*), and the content of small particles increases, as shown in figures 12(*d*)–(*i*).

The aspect ratio, area and diameter distribution functions are relative statistical parameters. The agreement of relative statistical parameters between simulation microstructures and actual microstructures can still not indicate completely that the simulation microstructures agree with actual microstructures. An additional absolute statistical parameter is required. In this work, the mean particle number density (the number of particles contained in a unit area) is adopted. Table 4 summarizes the mean particle number density of both simulated and experimental microstructures, and reveals that the particle number density of simulated microstructures can be controlled by the diameter distribution function. Simulation S2 has the best approximation.

According to both the relative and absolute statistical parameters, simulation S2 is the best approximation. The simulated S2 microstructure is shown in figure 13. It can be seen that the 3D realistic microstructure of PRMMC can be generated by controlling the simulation parameters α, $\boldsymbol{K}$ and the diameter distribution function of the primitive object. The simulated 3D realistic microstructure mimics the aspect ratio, area and diameter distribution functions of the actual microstructure, as well as the mean particle number density. Since the assessments of the effect of each simulation parameter on the simulated microstructure are the corresponding attributes of the algorithm, they can be reused for generating other realistic microstructures.

5.5. Discussion of the PRMMC microstructure model

The present algorithm permits simulations of virtual PRMMC microstructures that have different volume fractions. For example, figure 14 shows a simulated large virtual 3D

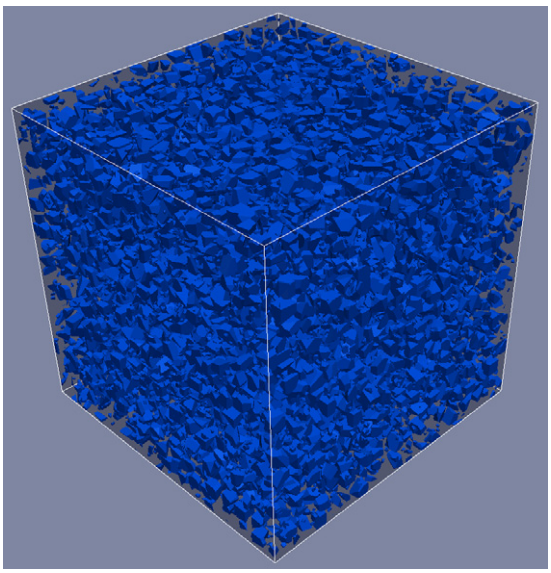

Figure 14. Simulated large 3D PRMMC microstructure with 15 vol% SiC particles which has the same SiC particle population as simulation S2.

microstructure, where all simulation parameters, except SVF, have been kept the same as simulation S2, for the composite reinforced by 15 vol% SiC particles.

In most actual composite manufacturing, the SiC, Al_2O_3, B_4C particles are polycrystalline. The facets of particles are not strict crystal faces, so there is no strict angle relationship between the facets of particles. In other words, the relationship between any two facets of particles is random. That is why we use random polyhedron to approximate particles. In real composites, the shapes of particles have camber concaves. However, the concave shape is not too serious, so with an admissible approximation, the concave-shaped surfaces are simplified to planar facets. An issue is that real composites reinforced by different particles may differ in the particle shape. For example, Al_2O_3 particles generally have a more spherical shape, while B_4C or SiC particles have a random polyhedral shape with sharp corners. The present microstructure simulation algorithm shows the ability to generate virtual microstructures with different particle shapes. It has been revealed that the simulated particle shape can be controlled by changing the simulation parameter(s) (α or/and $\boldsymbol{K}$). For example, figure 15 shows that the shape of most of the particles in simulation S4 is equiaxial polygonal, while the shape of most of the particles in simulation S6 is elongated polygonal. These virtual microstructures can be integrated in virtual investigations of PRMMC microstructure and design. If the microstructure-based evaluation of material properties is different from the specific target properties, modifications can be conducted in the microstructure simulation, which are then incorporated into the next material property evaluation. Such an inverse investigation is the core part of the virtual material design, which cuts down experimental costs such as time, resources and energy.

In the microstructure-based computations of material properties, the microstructure model must satisfy some quantitative criteria to represent the composite. Usually, the minimum size of the microstructure model is related closely to the purpose of the simulation in which the microstructure model is used [34]. Several studies have shown that the minimum sizes of a 2D microstructure model are $\delta = 16$ [35], $\delta = 24$ [36], $\delta = 50$ [34], where the dimensionless variable δ is called the size ratio, and is defined by the side length of the microstructure model L

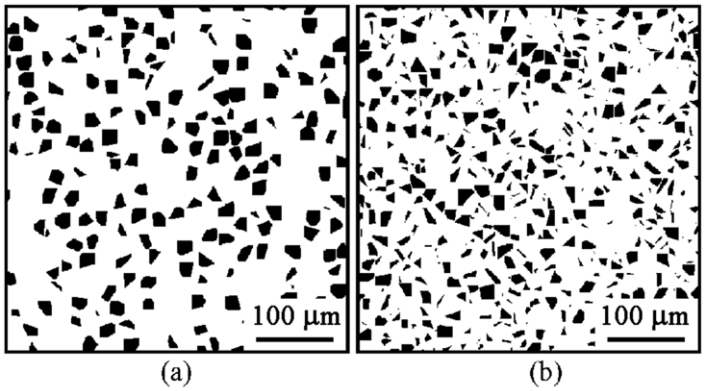

Figure 15. 2D microstructures of (*a*) simulation 4 and (*b*) simulation 6.

and the radius of reinforcement R using

$$\delta = \frac{L}{R}. \tag{11}$$

The minimum size of a 3D microstructure is a more complicated problem. Kanit *et al* [37] investigated the size of the microstructure model for 3D random composites. They showed that the minimum size of the 3D microstructure model depends on the specific values chosen for the material parameters of the different phases in the simulation. Furthermore, as Gitman *et al* [38] showed, the RVE sizes, which are realized in terms of the predicted macroscopic physical properties via homogenization, are dependent not only on the values of the material parameters, but also on the types of material behavior considered. The exception is that no RVE size may exist with the presence of localization deformation [38]. According to these 2D and 3D results, the ability to generate large 3D microstructures is important for the study of the minimum size problem.

Let us compute the size ratio of the 3D microstructures in figures 13(*a*) and 14. The side length of the 3D microstructures is 450 μm. The normal mean diameter of particles is 20 μm. Then the size ratio is computed to be 45 from equation (11).

In order to simulate realistic, high-quality 3D microstructures, reliable experimentally based data, which results from 3D characterization and quantitative analysis of real microstructures, is required, and can serve as model parameters to start direct modeling, or as reference parameters for inverse modeling. However, flexible and robust techniques for characterizing and quantitatively analyzing the main properties of the reinforcements in a 3D microstructure, such as size (diameter, surface area, volume, etc.), shape (random or not, isotropic or not, symmetric or not, etc.) and spatial arrangements (periodic or not, cluster or not, gradient or not, etc.), are still under development.

Recently, Tewari *et al* [39] proposed a practical technique based on two-point correlation functions that are governed implicitly by the properties of reinforcements in a 3D material. They developed a quantitative analysis method for estimating the microstructural attributes, especially the clustering behavior of particles in PRMMCs. This technique was then integrated into large realistic 2D microstructure modeling and the medium realistic 3D microstructure modeling of PRMMCs, respectively, by Singh *et al* [6] and Mao [8], using a digital image process-based cell decomposition geometry modeling technique. Chord length distribution (CLD) reflects the sizes, shapes and spatial arrangements of geometrical particles [40], and is, therefore, also an important objective measurement for the quality of the generated microstructure. CLDs can be estimated from small-angle scattering data [41, 42]. This is future

aim of the model. Once two-point correlation functions or the CLD method are implemented for the quantitative analysis of the 3D BREP model, it is possible to simulate 3D realistic material with more complex microstructures, by matching the same estimated properties with experimental PRMMC microstructures, like the statistically reconstructed 2D microstructure proposed by Rintoul and Torquato [43].

In this work, traditional 2D quantitative metallographic methods are applied, to estimate the size and shape of the sections of a 3D material. It is important to recognize that the microstructure parameters, estimated by 2D sections, may involve errors, especially when the microstructure has quite complex attributes, such as clustering, directional arrangement and layer arrangement. Nonetheless, the present work focuses on modeling microstructures using the BREP technique, to achieve planar approximations of the reinforcement boundaries, and has modeled the PRMMC microstructures with uniformly distributed particles successfully by using a cuboid as the primitive object. This 3D model is flexible enough to permit large simulations with complex attributes. This may be the first contribution that integrates the BREP technique for the 3D realistic microstructure simulation of PRMMCs. The BREP technique allows the direct calculation of the surface area of polyhedrons, because all the sides of polyhedrons are planar, and all the vertices are known. It is useful for understanding the reinforcement-matrix bonding properties in PRMMCs.

During the present RSA algorithm, the rotational DOF of geometrical particles is not used. If the rotational DOF is activated in the RSA, the anisotropy properties of 3D microstructures generated with $\alpha > 1.0$ would be removed. Besides, using or not using the rotational DOF will have significant effects on the possible microstructures achieved, considering microstructures where particles are less spherical, or microstructures with maximal possible particle SVFs. This then, in turn, may influence the global material behavior obtained by the microstructure-based material property simulations.

6. Conclusions

(1) A new and robust methodology is developed for computer simulations of large 3D PRMMC microstructures, that can be used for virtual investigation of PRMMC structure and design. The size and shape of the reinforcements can be controlled by the simulation parameters α and $\boldsymbol{K}$, as well as the diameter distribution function.

(2) By increasing the simulation parameters α and $\boldsymbol{K}$, the mean aspect ratio of simulated particles increases, and the mean size of the simulated particles decreases.

(3) The variation of the size of primitive objects has little effect on the aspect ratio of the simulated particles, but has a significant effect on the size of the simulated particles. The mean size of the simulated particles decreases with decreasing the size of the primitive objects.

(4) The methodology can be applied for computer simulations of large 3D realistic microstructures that mimic the distribution functions of aspect ratio, diameter and area of reinforcement of real microstructures. The methodology is general, extensible and applicable for simulating complex PRMMC microstructures.

Acknowledgment

The authors gratefully acknowledge the support of the National Basic Research Program of China under grant No 2012CB619600.

References

[1] Povirk G L, Stout M G, Bourke M, Goldstone J A, Lawson A C, Lovato M, Macewen S R, Nutt S R and Needleman A 1992 Thermally and mechanically induced residual strains in Al–SiC composites *Acta Metall. Mater.* **40** 2391–412

[2] Tszeng T C 1998 The effects of particle clustering on the mechanical behavior of particle reinforced composites *Composites* B **29** 299–308

[3] Mishnaevsky L L Jr 2004 Three-dimensional numerical testing of microstructures of particle reinforced composites *Acta Mater.* **52** 4177–88

[4] Li M, Ghosh S, Richmond O, Weiland H and Rouns T N 1999 Three dimensional characterization and modeling of particle reinforced metal matrix composites: II. Damage characterization *Mater. Sci. Eng.* A **266** 221–40

[5] Singh H, Mao Y, Sreeranganathan A and Gokhale A M 2006 Application of digital image processing for implementation of complex realistic particle shapes/morphologies in computer simulated heterogeneous microstructures *Modelling Simul. Mater. Sci. Eng.* **14** 351–63

[6] Singh H, Gokhale A M, Mao Y and Spowart J E 2006 Computer simulations of realistic microstructures of discontinuously reinforced aluminum alloy (DRA) composites *Acta Mater.* **54** 2131–43

[7] Mao Y, Gokhale A M and Harris J 2006 Computer simulations of realistic microstructures of coarse constituent particles in a hot-rolled aluminum alloy *Comput. Mater. Sci.* **37** 543–56

[8] Mao Y 2010 Computer simulations of realistic three-dimensional microstructures *PhD Thesis* Georgia Institute of Technology

[9] Chawla N, Ganesh V V and Wunsch B 2004 Three-dimensional (3D) microstructure visualization and finite element modeling of the mechanical behavior of SiC particle reinforced aluminum composites *Scr. Mater.* **51** 161–5

[10] Chawla N, Sidhu R S and Ganesh V V 2006 Three-dimensional visualization and micro structure-based modeling of deformation in particle-reinforced composites *Acta Mater.* **54** 1541–8

[11] Landis E N and Keane D T 2010 X-ray microtomography *Mater. Charact.* **61** 1305–16

[12] Kenesei P, Borbely A and Biermann H 2004 Microstructure based three-dimensional finite element modeling of particulate reinforced metal–matrix composites *Mater. Sci. Eng.* A **387** 852–6

[13] Borbely A, Csikor F F, Zabler S, Cloetens P and Biermann H 2004 Three-dimensional characterization of the microstructure of a metal–matrix composite by holotomography *Mater. Sci. Eng.* A **367** 40–50

[14] Padilla E, Jakkali V, Jiang L and Chawla N 2012 Quantifying the effect of porosity on the evolution of deformation and damage in Sn-based solder joints by x-ray microtomography and microstructure-based finite element modeling *Acta Mater.* **60** 4017–26

[15] Williams J J, Yazzie K E, Padilla E, Chawla N, Xiao X and De Carlo F 2013 Understanding fatigue crack growth in aluminum alloys by *in situ* x-ray synchrotron tomography *Int. J. Fatigue* **57** 79–85

[16] Widom B 1966 Random sequential addition of hard spheres to a volume *J. Chem. Phys.* **44** 3888–94

[17] Coelho D, Thovert J F and Adler P M 1997 Geometrical and transport properties of random packings of spheres and aspherical particles *Phys. Rev.* E **55** 1959–78

[18] Bohm H J, Eckschlager A and Han W 2002 Multi-inclusion unit cell models for metal matrix composites with randomly oriented discontinuous reinforcements *Comput. Mater. Sci.* **25** 42–53

[19] Torquato S 2002 *Random Heterogeneous Materials: Microstructure and Macroscopic Properties* (New York: Springer)

[20] Williams S R and Philipse A P 2003 Random packings of spheres and spherocylinders simulated by mechanical contraction *Phys. Rev.* E **67** 051301

[21] Tu S T, Cai W Z, Yin Y and Ling X 2005 Numerical simulation of saturation behavior of physical properties in composites with randomly distributed second-phase *J. Compos. Mater.* **39** 617–31

[22] Gusev A A 1997 Representative volume element size for elastic composites: a numerical study *J. Mech. Phys. Solids* **45** 1449–59

[23] Manwart C and Hilfer R 1999 Reconstruction of random media using Monte Carlo methods *Phys. Rev.* E **59** 5596–9
[24] Galli M, Botsis J and Janczak-Rusch J 2008 An elastoplastic three-dimensional homogenization model for particle reinforced composites *Comput. Mater. Sci.* **41** 312–21
[25] Fritzen F and Bohlke T 2011 Periodic three-dimensional mesh generation for particle reinforced composites with application to metal matrix composites *Int. J. Solids Struct.* **48** 706–18
[26] Si H 2008 Three dimensional boundary conforming Delaunay mesh generation *PhD Thesis* Technische Universität Berlin
[27] Miller G L, Talmor D, Teng S H, Walkington N and Wang H 1996 Control volume meshes using sphere packing: generation refinement, and coarsening *Proc. 5th International Meshing Roundtable* (Albuquerque, NM: Sandia National Laboratories)
[28] Belytschko T, Parimi C, Moes N, Sukumar N and Usui S 2003 Structured extended finite element methods for solids defined by implicit surfaces *Int. J. Numer. Methods Eng.* **56** 609–35
[29] Sethian J A and Wiegmann A 2000 Structural boundary design via level set and immersed interface methods *J. Comput. Phys.* **163** 489–528
[30] Ian S 2006 *Boundary Representation Modelling Techniques* (Heidelberg: Springer)
[31] Kari S, Berger H and Gabbert U 2007 Numerical evaluation of effective material properties of randomly distributed short cylindrical fibre composites *Comput. Mater. Sci.* **39** 198–204
[32] Pan Y, Lorga L and Pelegri A A 2008 Numerical generation of a random chopped fiber composite RVE and its elastic properties *Compos. Sci. Technol.* **68** 2792–8
[33] Pan Y, Lorga L and Pelegri A A 2008 Analysis of 3D random chopped fiber reinforced composites using FEM and random sequential adsorption *Comput. Mater. Sci.* **43** 450–61
[34] Trias D, Costa J, Turon A and Hurtado J E 2006 Determination of the critical size of a statistical representative volume element (SRVE) for carbon reinforced polymers *Acta Mater.* **54** 3471–84
[35] Khisaeva Z F and Ostoja-Starzewski M 2006 On the size of RVE in finite elasticity of random composites *J. Elast.* **85** 153–73
[36] Liu C 2005 On the minimum size of representative volume element: An experimental investigation *Exp. Mech.* **45** 238–43
[37] Kanit T, Forest S, Galliet I, Mounoury V and Jeulin D 2003 Determination of the size of the representative volume element for random composites: statistical and numerical approach *Int. J. Solids Struct.* **40** 3647–79
[38] Gitman I M, Askes H and Sluys L J 2007 Representative volume: existence and size determination *Eng. Fract. Mech.* **74** 2518–34
[39] Tewari A, Gokhale A M, Spowart J E and Miracle D B 2004 Quantitative characterization of spatial clustering in three-dimensional microstructures using two-point correlation functions *Acta Mater.* **52** 307–19
[40] Li M Z and Wilkinson D 2005 Determination of non-spherical particle size distribution from chord length measurements: I. Theoretical analysis *Chem. Eng. Sci.* **60** 3251–65
[41] Gille W 2000 Chord length distributions and small-angle scattering *Eur. Phys. J.* B **17** 371–83
[42] Hansen S 2003 Estimation of chord length distributions from small-angle scattering using indirect Fourier transformation *J. Appl. Crystallogr.* **36** 1190–6
[43] Rintoul M D and Torquato S 1997 Reconstruction of the structure of dispersions *J. Colloid Interface Sci.* **186** 467–76